CrystEngComm

Accepted Manuscript

ROYAL SOCIETY OF CHEMISTRY

www.rsc.org/crystengcomm

Seedless growth of ZnO nanorods on TiO_2 fibers by chemical bath deposition

Benxue Liu, Cong Feng, Xingshuang Zhang, Luyi Zhu*, Xinqiang Wang, Guanghui Zhang, Dong Xu*

State Key Laboratory of Crystal Materials and Institute of Crystal Materials, Shandong University, Jinan 250100, PR China

Corresponding authors

E-mail addresses: zhuly@sdu.edu.cn (Luyi Zhu) xdoffice@sdu.edu.cn (Dong Xu)

Abstract

Chemical bath deposition method without using ZnO seed layers was developed to grow dense ZnO nanorods (NRs) on TiO_2 fibers under the saturated nutrition solution. The crystal phase, microstructure and photoluminescence of the as received heterostructure were examined using X-Ray Diffraction (XRD), Scanning-electron microscopy (SEM), Transmission electron microscopy (TEM), Energy-dispersive X-ray spectroscopy (EDX) and Photoluminescence spectra (PL). The structure consists of TiO_2 fibers core and radial ZnO NRs shell of which growth directions are almost perpendicular to the central fibers. The luminescence quenching of TiO_2 was observed in the PL spectra of the heterostructure due to the shield effect of the covered ZnO NRs. According to the results of SEM, XRD, Infrared spectra (IR), EDX, the seedless growth mechanism was discussed. It was found that, at room temperature, Zn-base layer double hydroxides (Zn-LDHs) with positive charges were firstly formed in ZnO growth solution, which are the build block for the nucleation and growth of ZnO NRs. The Zn-LDHs were deposited on the negatively charged TiO_2 fibers through electrostatic attraction followed by being dehydrated into ZnO NRs in elevated temperature. The cooperative interaction between TiO_2 fibers and ZnO NRs was investigated. The two-component in the structure has a robust interaction that violent ultrasonic power could not peel off the ZnO NRs from the TiO_2 fibers.

Introduction

The ever-growing research interest in one-dimensional (1D) ZnO nanostructures is motivated by their emerging applications in optoelectronic devices [1], photovoltaic devices [2], photocatalysts [3] and nanogenerators [4] due to the wide band gap of 3.37eV, high electron mobility, piezoelectricity, and high thermal and air stability. Well-aligned 1D ZnO nanoarrays grown on substrates can be achieved through a variety of paths such as metal organic chemical vapor deposition [5], thermal evaporation [6], molecular beam epitaxy [7], metal organic vapor phase epitaxy [8], solution-base method [9], etc. Among them, solution base methods including chemical bath deposition and hydrothermal method are of particular interest because of the low-cost, low reaction temperature, environmental friendliness, and ease of scaling up. However, the approaches usually require seed layers composed of packed ZnO nanocrystals acting as nucleation sites upon which ZnO NRs could be grown. Although high quality ZnO nanostructures are promised, sophisticated steps are required which would increase the cost. Under some circumstances, the disordered polycrystalline ZnO seeds may hinder facile carrier transport between NRs and substrates, which is critical for utilizing [10].

In recent years, strenuous efforts have been devoted to seedless growth of 1D ZnO nanostructures [11]. In terms of classical crystal growth theory, the process could be summarized into nucleation of primary nucleus on substrates which is the most challenged due to the large nucleation barrier and the followed growth through stacking of growth units. Strategies such as single crystalline substrates with low lattice mismatch to ZnO [12], Au seed layer [13] and applied electrical field on target substrate [14] are developed to decrease the nucleation energy. However, these are mostly focused on the growth on flat rigid substrates. Fibrous material with high surface area and large aspect ratio is a category of flexible substrates. The fiber base 1D ZnO nanostructure is a vital candidate in portable nanogenerator [4] and electrochemical anode [15].

In this work, seedless growth of ZnO NRs on TiO_2 fibers using chemical bath deposition was reported. The microstructure and growth process were studied to uncover the seedless growth mechanism. The morphology of the interface between fibers and NRs was investigated with the assistant of TEM and HRTEM. At last, the samples dispersed in water endure violent ultrasonic to investigate whether the NRs have a high adhesive strength with to the fibers.

2. Experimental

2.1. Chemicals and materials.

Titanium tetrachloride ($TiCl_4$, ≥99.0%), acetylacetone (Hacac, ≥98.0%), triethylamine (TEA, ≥99.0%),

tetrahydrofuran (THF, ≥99.0%), anhydrous methanol (CH_3OH, ≥99.5%), zinc nitrate hexahydrate ($Zn(NO_3)_2·6H_2O$, ≥99.0 %), hexamethylenetetramine (HMTA, ≥99.0 %), deionized water (DI water, 18.2 MΩ).

2.2. Fabrication of the TiO_2 fibers.

Generally, TiO_2 fibers were fabricated by force-spinning spin dopes of a concentrated organotitanium methanol solution into precursor fibers followed by heat treatment. The organotitanium compound was synthesized according to previously reported [16]. For simplicity, the synthesis was introduced in supporting information. In spinning process, 30 g as-obtained organotitanium compound was dissolved in 100 ml of methanol with vigorous magnetic stirring, and then the solution was concentrated into a certain viscosity using vacuum rotator evaporator under a condition of -0.1 mbr, 40 ºC. The viscous spin dopes were spun into precursor fibers using centrifugal spinning device. The detailed spinning parameters were listed in Table S1. After that, the precursor fibers were transformed into TiO_2 crystalline fibers by heat treatment. The characterizations of the TiO_2 fibers were shown in Fig. S2 (Photo image and XRD pattern of the TiO_2 fibers heat-treated at 500 ºC).

2.3. Growth of ZnO NRs on TiO_2 fibers.

Equimolar aqueous solutions of $Zn(NO_3)_2·6H_2O$ and HMTA were used to grow ZnO NRs. First, 0.025 M (0.876 g) HMTA was prepared in 250 ml of DI water. Once completely dissolved, 1.859 g $Zn(NO_3)_2·6H_2O$ was added into the above solution, which was followed by stirring for 24 h. A turbid solution for the growth of ZnO was obtained (pH=6~7). 0.1 g TiO_2 fibers were weighed and immersed into the ZnO growth solution, which was placed in chemical bath at 70 ºC for 4 h. After that, the fibers were separated with rinsing three times by DI water. The samples contain ZnO NRs-TiO_2 fibers heterostructure were obtained after dried in air (denoted as ZnO-TiO_2 after all).

2.4. Measurements.

The X-ray diffraction (XRD) patterns of samples were collected on a Bruker AXSD8 Advance X-ray diffractometer with Cu Kα radiation using a graphite chromator. Diffraction peaks were record in the 10-80° (2θ) range with a step size of 0.02°.The morphologies and microstructures of the samples were characterized using a Hitachi S-4800 scanning electron microscope (SEM) instrument. Transmission electron microscopy (TEM) images were record using a JEM-200CX electron microscope operating at 20 kV. The infrared (IR) spectra were measured on a Nicolet 5DX-FTIR spectrometer using KBr pellet method in the range of 4000-375 cm^{-1}. Zeta potential of ZnO growth solution and TiO_2 fibers aqueous solution was determined by Brookhaven Instruments ZetaPALS DB-525. The photoluminescence (PL) spectra of the samples at room temperature were measured on

ground powders with an Edinburgh Instruments FLS920 fluorescence spectrometer equipped with an ANDO Shamrock SR-303i high-resolution optical spectrum analyzer and a tunable Opolette (HE) 355 Ⅱ (5 ns, 20 Hz) pump source.

3. Results and Discussion

3.1. Characterizations of the ZnO-TiO_2 heterostructure.

XRD, SEM, and the corresponding EDX spectra were used to characterize the obtained ZnO-TiO_2 heterostructure, and the results are shown in Fig. 1. From Fig. 1a, the fibers, heat-treated at 500 °C, present continuously long morphology and the average diameter was around 8.67 μm as shown in Fig. 1c. The inset in Fig. 1a is a magnified view of the individual TiO_2 fiber surface. Smooth surface without secondary structure could be discerned clearly. After chemical bath deposition, it could be seen from Fig. 1b that the TiO_2 fibers were compactly muffled by a large number of ZnO NRs. The ZnO NRs were hexagonal in shape as indicated in Fig. S2. Moreover, the EDX spectrum of the structure (Fig. 1d) shows that O, Ti, Zn existed in the ZnO-TiO_2 heterostructure, whereas only O, Ti elements existed in the pristine TiO_2 fibers theoretically. The C peaks are attributed to the adhesive tapes used to support the samples on the SEM platform. The diffraction peaks of the sample are shown in Fig. 1e. As for the pattern of the sample, diffraction peaks at about 2θ= 25.3°, 36.9°,48.4°,53.9, 55.1°,62.8° 69.8°, 70.3°, 75.0° could be indexed to the (101), (004), (200), (105), (211), (204), (116), (220), (215) crystal facets of anatase TiO_2 (JCPDS 21-1271), respectively. Besides, additional diffraction peaks with 2θ values of 31.8°, 34.4°, 36.2°, 56.6°, 68.0° were appeared corresponding to (100), (002), (101), (110), (112) crystal facets of wurtzite phase ZnO (JCPDS 36-1451), respectively.

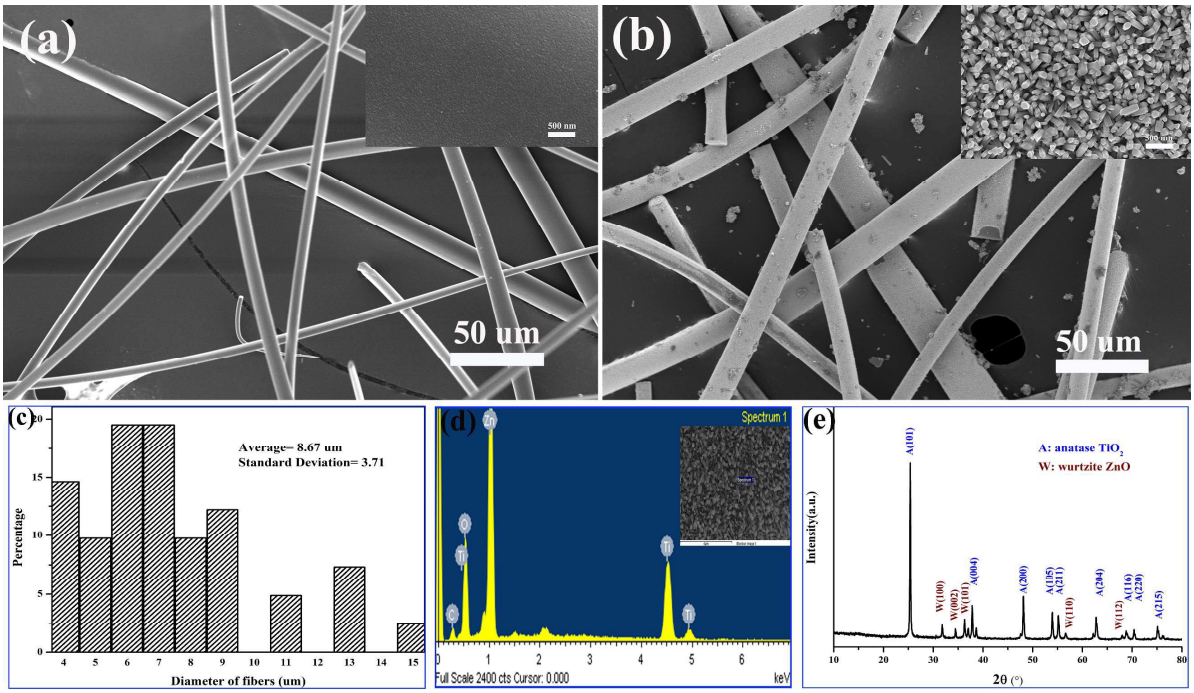

Fig. 1. SEM images of (a) pristine TiO_2 fibers and (b) ZnO-TiO_2 heterostructure, the insets are the magnified images of fiber surface. (c) Diameter distribution statistics of TiO_2 fibers, (d) EDX spectra and (d) XRD patterns of ZnO-TiO_2 heterostructure.

To further clarify the ZnO-TiO_2 heterostructure, TEM and HRTEM measurements were performed and the results are shown in Fig. 2. As observed in Fig. 2a, highly dense ZnO NRs standing over the TiO_2 fiber surface, exhibited a branching structure, and the top of the ZnO NRs appeared rugged morphology. It is coincided with the results from the SEM observations shown in Fig. 2a inset. The image further shows that the ZnO NRs possess a diameter of about 100 nm. Fig. 2b displays HRTEM image of an individual ZnO NRs, and the interplanar distance of ca. 0.28 nm is consistent with the d-spacing of the (100) plane of the wurtzite ZnO. The fast Fourier transform (FFT) of the diffractogram from a region framed by the red square in Fig. 2b again shows a single crystal-type zone-axis pattern. We proceed to visualize the interface of ZnO-TiO_2 with HRTEM, and the results shown in Fig. 2d. Although the polycrystalline seed layer is commonly observed in conventional epitaxial growth of 1D ZnO [11], it seems absent in this research. The observed neat interface between ZnO and TiO_2 indicates the heterogeneous growth of ZnO NRs on TiO_2 fibers unambiguously, whereas the growth using seed layer is homogeneous growth substantially. Two types of lattice fringes were observed in the image. One type of the fringes spacing was ca. 0.35 nm, corresponding to the (101) plane of anatase TiO_2. Another type of the fringes spacing measured ca. 0.26 nm, corresponding to the (001) plane of wurtzite ZnO.

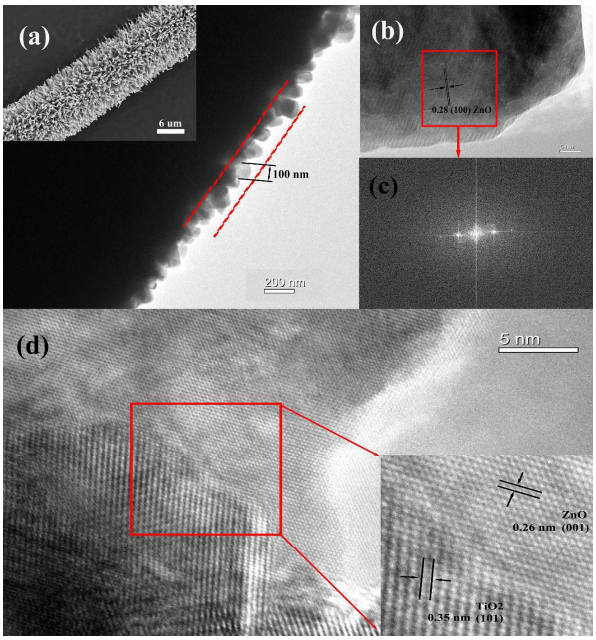

Fig. 2. (a) TEM image of ZnO-TiO_2 heterostructure, the inset was SEM image of individual TiO_2 fiber covered by ZnO NRs. (b) HRTEM image of ZnO NRs and (c) FFT diffractograms of the selected area (d) HRTEM image of ZnO-TiO_2 interface.

3.2. Time-dependent crystal growth process.

Time-dependent experiments were performed to understand the seedless formation mechanism of the ZnO NRs on TiO_2 fibers. The evolution of the heterostructure for ZnO NRs on the TiO_2 fiber surface was characterized by SEM. As shown in Fig. 3a, the surface of pristine TiO_2 fiber was smooth without secondary structure. After chemical bath depositing in ZnO growth solution for 30 min (Fig. 3b), the surface of the fiber was compactly covered by a layer of wrinkled lamina with irregular shape. The wrinkle is so thin that the particle profile on fiber surface could be observed through the penetrable electron beam. With the reaction time extending to 2 h, a mixture of the lamellar structures and hexagonal rods was observed together. The NRs were grown in a direction, which was almost perpendicular to the lamina. When the reaction time was further extended to 4 h, it could be observed that the hexagonal rods became the prominent structures and the laminae were gradually transformed into NRs completely.

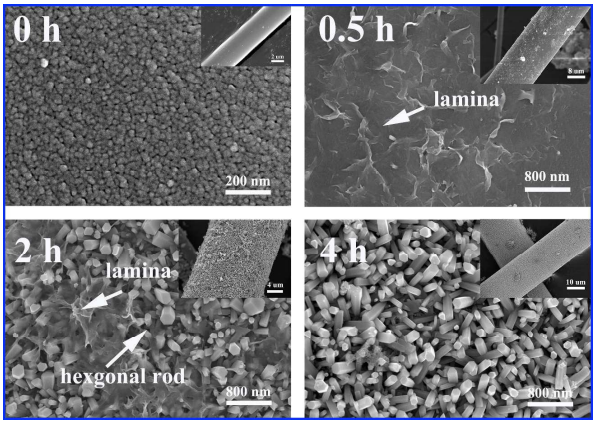

Fig. 3 SEM images of ZnO-TiO_2 heterostructure at various growth stages

To reveal the nature of the lamina, XRD, IR, SEM were performed. Owning to low content of the laminae on the fibers, extension of stirring time of the ZnO growth solution was conducted to gain enough laminae for characterization. After stirring for 48 h at room temperature, sufficient white precipitates could be isolated from the growth solution. As shown in Fig. 4a, SEM images of the precipitates present a lamellar structure. However, unlike the wrinkle on the surface of the fibers (Fig. 4b), the laminae had a serious aggregation due to high surface energy. EDX spectra were used to characterize the laminae attached on fibers. As shown in Fig. 4c, Zn, Ti, O, C and N elements were detected on the surfaces of the TiO_2 fibers. It indicates that the lamina is a Zn-based compound derived from ZnO growth solution. Further careful analysis of the precipitates using XRD (Fig. 4c) shows that the pattern matched well with zinc hydroxide nitrate, namely $Zn_5(OH)_8(NO_3)_2 \cdot 2H_2O$, which has been reported in the literature [17] (denoted as Zn_5 after all). Fig. 4e shows the IR spectra of the precipitates. The absorption peaks of main functional groups in Zn_5 such as -OH, NO_3^-, and H_2O were detected, which further determines the identity of the lamina.

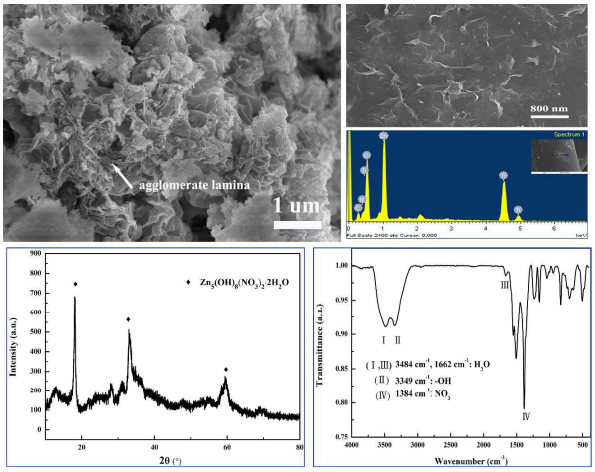

Fig. 4. (a) SEM image of the lamina incubated in growth solution and (b) absorbed on fiber surface. (c) EDX spectra of the lamina absorbed on fiber surface. (d) XRD pattern and (e) IR spectrum of the lamina incubated in ZnO growth solution.

At elevated temperatures, Zn_5 could transform into ZnO through multistep pathway involving structure and compositional transformation[18, 19]. For the purpose of excluding the influence of TiO_2 fibers on the transformation in our research, after the first stage of incubation of Zn_5 at room temperature, the evolution of ZnO NRs homogeneously grown in growth solution at identical temperature is monitored by SEM and XRD. After chemical bath for desired duration, the precipitation was isolated through centrifuging from growth solution for observation. As discussed in Fig 4a, the Zn_5 was laminar precipitation. After chemical bath for 1h, from Fig. 5a, it could be seen that rod-like structures are penetrated through the lamina. For convenient observation, the rods are circled by red color. Such an outgrowth of NRs from Zn_5 indicates the Zn_5 could transform into NRs through solid-solid transformation. The XRD patterns shown in Fig. 5b only demonstrate the existence of ZnO after chemical bath for 1h, which means that the lamina are no longer the Zn_5. A broad band between 20° and 30° circled by red color was detected. It was assumed that the Zn_5 may transform into amorphous species at elevated temperature. With the increase of duration, from the observation of the isolation, the lamina gradually decreased in the view. In contrast, NRs prevail. This is attributed to the gradual transformation of Zn_5 to ZnO. The XRD patterns also present single wurtzite ZnO phase. The amorphous species were disappeared as the time increasing. It should be noted that the NRs homogeneously grown in growth solution are poor uniform in compared with those heterogeneously grown on TiO_2 fibers. It would be analyzed in next part.

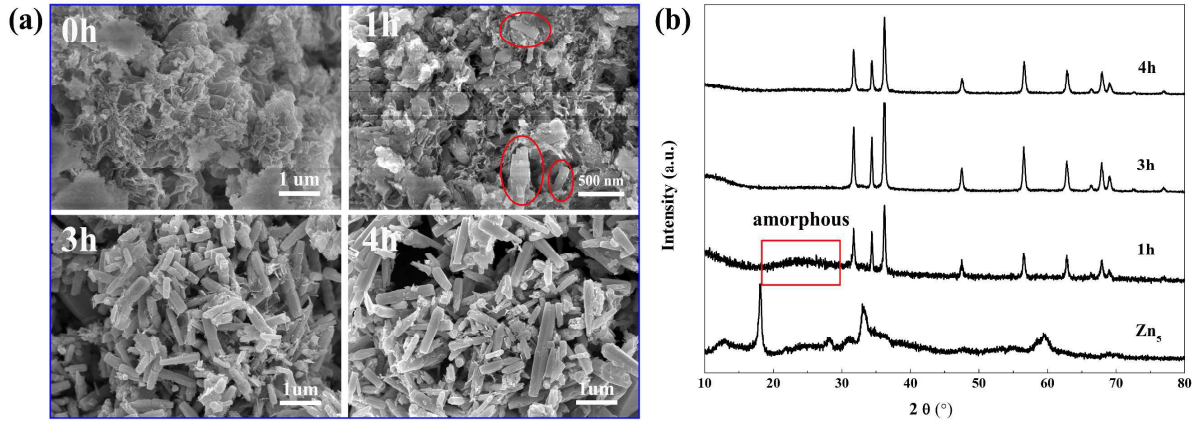

Fig. 5 (a) SEM images and (b) XRD patterns of ZnO NRs homogeneously grown in growth solution at various stages

3.3. Growth mechanism

Based on the above results, the growth mechanism was proposed to explain the seedless formation of ZnO NRs on TiO_2 fibers. Fig. 6a demonstrates the process of adsorption of Zn_5 on fiber surface. The surfaces of TiO_2 fibers consist of unsaturated coordination Ti^{4+} and O^{2-} due to the crystalline nature, and are usually terminated by OH groups in order to reduce the coordinative unsaturation. When TiO_2 fibers were immersed in ZnO growth solution (pH=6~7), the fiber surfaces became electronegative as demonstrated by zeta potential shown in the inset of Fig.S3 due to the reaction between surface absorbed OH groups and the aqueous solution. It should be noticed that the OH groups could react with both H^+ and OH^-. As a result, the fiber surfaces are either electronegative or electropositive in terms of the pH value of the aqueous solution. In the meantime, a Zn-base layer double hydroxide (Zn-LDH), Zn_5, with positive charge was formed (equation 1) in growth solution which has been reported in many researches that it is an intermediate product in the synthesis of ZnO NRs [20]. Owning to electrostatic attraction between opposite charges, the Zn_5 could be easily absorbed on the surfaces of TiO_2 fibers.

After absorbed onto fiber surface, Zn_5 has tendency to transform into ZnO at elevated temperature due to the reduction of free energy. From Fig. 5, the penetrating ZnO NRs through Zn_5 indicates an in situ solid-solid transformation. However, according to the reference, Zn_5 is thermal stable up to about 110 ºC [17]. It could be deduced that the elevated temperature itself does not directly decide the transition. For better understand the transition mechanism of Zn_5 to ZnO, the crystal structures of Zn_5 and ZnO (Fig. 6b) were carefully studied. The Zn_5 consists of periodic Zn-O polyhedron layers and intercalated nitrate anions which are easily substituted by other anions via ions exchange reaction [21]. In our research, the HMTA was used to provide OH^- through decomposition which can be expressed as equation 2. Elevation of the reaction temperature could increase the rate of HMTA decomposition, facilitating the release of OH^- groups. At this stage, the Zn_5 may have undergone anion substitution to form $Zn(OH)_2$ (equation 3) which then dehydrated to ZnO (equation 3). $Zn(OH)_2$ has been proved to has possibility to transform into ZnO at low temperature [22]. Amorphous $Zn(OH)_2$ may be the origin of the broad band in Fig. 5b. The following stacking of growth units upon the initial NRs on fiber surface could lead to the dense NRs array. It seems that the NRs grown on fibers are more uniform than that grown homogeneously in growth solution. It could be explained as follows: after initial nucleation on a fixed site on fiber surface, the growth of ZnO NRs is confined by substrate that only the growth perpendicular to fibers is allowed, whereas the homogeneous growth of NRs in solution is free that some nonclassical crystal growth process, such as oriented attachment [23], can occur. As demonstrated by Fig. S4, the ZnO NRs grown homogenously in growth solution were

poor uniform due to the oriented attachment.

$$5Zn^{2+} + 8OH^- + 2NO_3^- + 2H_2O \rightarrow Zn_5(OH)_8(NO_3)_2 \cdot 2H_2O \quad (1)$$

$$C_6H_{12}N_4 + 6H_2O \rightarrow 6HCHO + 4NH_3$$
$$NH_3 + H_2O \rightarrow NH_4^+ + OH^- \quad (2)$$

$$Zn_5(OH)_8(NO_3)_2 \cdot 8H_2O + 2OH^- \rightarrow 5Zn(OH)_2 + 2NO_3^- + 8H_2O \quad (3)$$

$$Zn(OH)_2 \rightarrow ZnO + H_2O \quad (4)$$

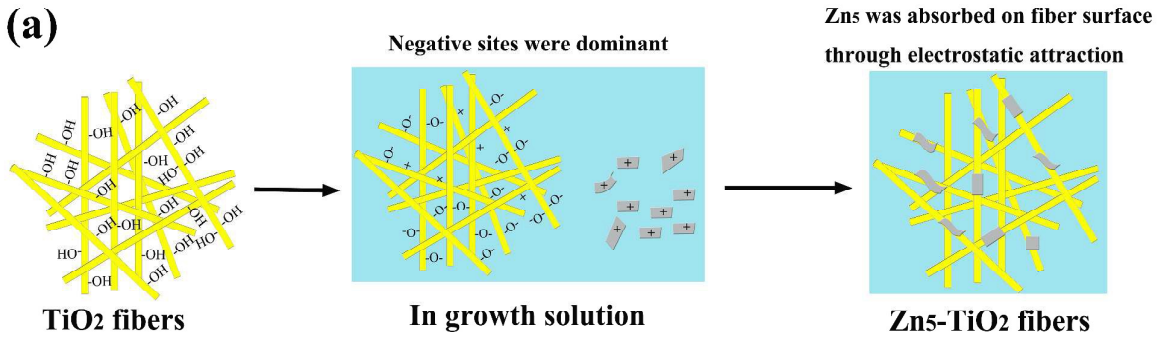

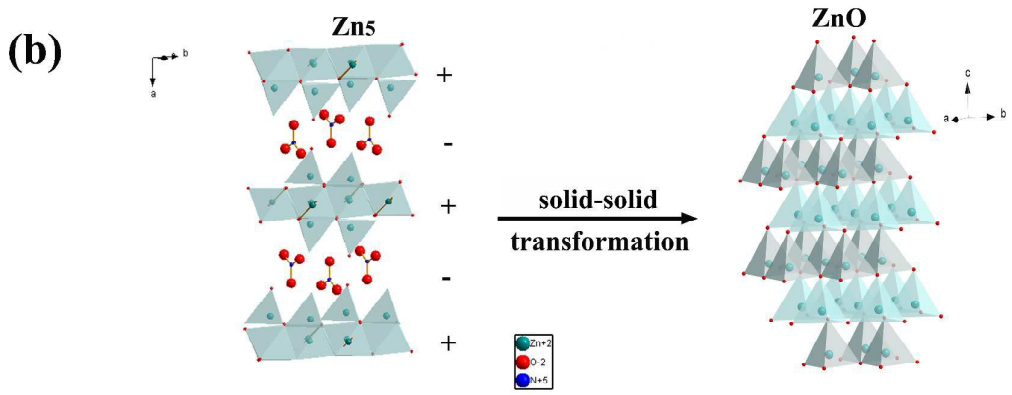

Fig. 6 Schematic of the seedless formation process of ZnO NRs on TiO_2 fibers

3.4. Stability of the ZnO NRs on TiO_2 fibers.

The interactions between ZnO nanostructures and substrates need considerations in particular because weak interactions would be likely to cause the nanostructures to be peel off if the samples are exposed to certain force field, such as sonication [3, 24]. As a result, performance reduction or even failure of the fabricated device is inevitable. For evaluating the stability of the as prepared ZnO-TiO_2 heterostructure in our research, the samples were dispersed in DI water followed by violent ultrasonic processing in an ultrasonic cleaner machine (Power: 150 W, Frequency: 40 kHz). The morphology changes of the structures were recorded by SEM shown in Fig. 6.

As can be seen in Fig. 6a, ZnO twinning NRs randomly distributed on the fibers were washed away through ultrasonic power. The twinning NRs were formed through homogeneous nucleation. Whereas the ZnO NRs grown on fiber surface through heterogeneous nucleation were stably anchored on fiber surfaces after ultrasonic processing for even 1 h. The magnified images shown in lower row indicate the ZnO NRs on fiber surfaces were still dense with hexagonal shape. The NRs gradually turned into hollow tube, which resulted from the dissolution of high energy crystalline facet of (001) [25]. All in all, the ZnO NRs show a robust interaction with fiber surfaces that ensure the integration could survive in flow, stirring and milling in applications.

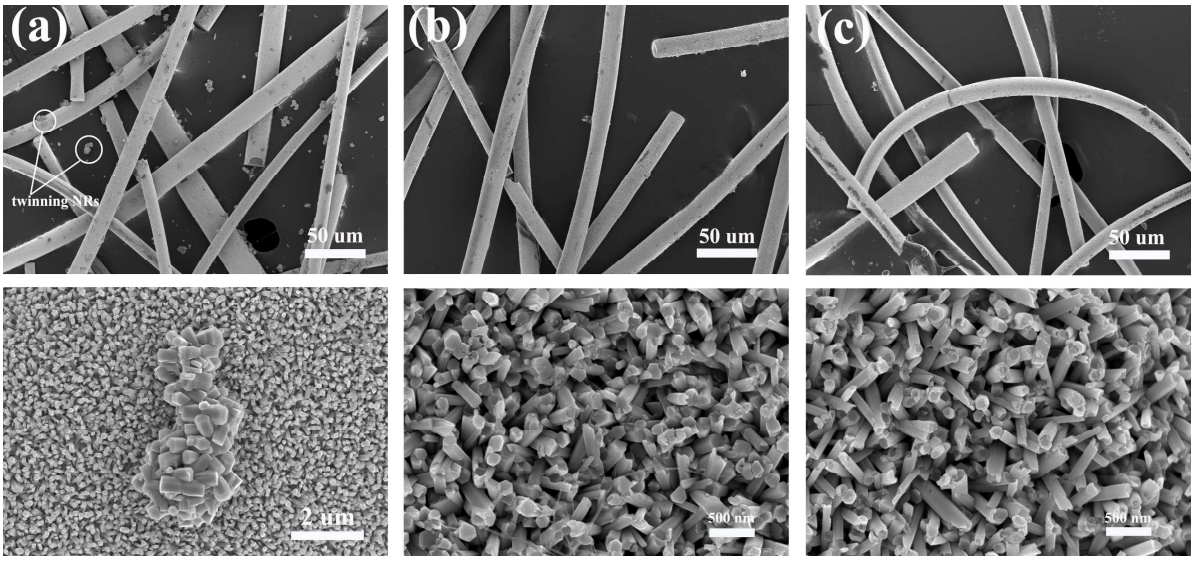

Fig. 7 SEM images of (a) ZnO-TiO_2 heterostructure and (b) endure ultrasonic processing for 30 min (c) 60 min. The lower row is magnified images of ZnO NRs anchored on fiber surfaces.

3.5. PL spectra of the ZnO-TiO_2 heterostructure.

Physical properties of a given materials, such as electricity, optics, magnetism, decided the fabricated device performance. These properties are highly correlated with crystalline quality and defect states which can be characterized by PL spectra. In our experiment, the PL spectra of the TiO_2 fibers, ZnO-TiO_2 heterostructure and ZnO NRs homogeneously grown from growth solution were investigated. As can be seen in Fig. 8a, the initial TiO_2 fibers show visible luminescence band centered at about 420 and 500 nm and near-infrared luminescence band centered at about 803 nm. The curve fitting shown in Fig. 8b presents the elaborated band structure. The luminescence band located at 417 nm is related to the self-trapped excitons, and the left bands are associated to oxygen vacancies and surface states [26]. According to literature, the near-infrared luminescence is attributed to rutile TiO_2 [27]. However, only anatase TiO_2 is investigated through XRD shown in Fig. 1 and Fig. S1. It is may be

due to the low content of the rutile phase in the synthesized TiO_2. After ZnO NRs deposition, the PL peaks from TiO_2 are almost disappeared. Such a luminescence quenching can be attributed to the shield effect of the covered ZnO NRs shell [28]. The emerging bands in ZnO-TiO_2 samples locate in 576 nm with a shoulder peak at 681 nm. It may derive from the ZnO NRs grown on TiO_2 fibers. For the purpose of excluding the origin of luminescence from TiO_2, the PL spectra of ZnO NRs homogeneously grown in growth solution were measured. The profiles of the peaks are similar with that of ZnO-TiO_2 heterostructure. The almost identical curving fitting results of PL spectra of ZnO-TiO_2 heterostructure and ZnO NRs also confirm the PL spectra of ZnO-TiO_2 heterostructure come from the ZnO NRs covered on TiO_2 fibers. It was well known that ZnO is direct band gap semiconductor that the band edge luminescence could be observed at about 380 nm [29]. However, in our research, the emission could not be observed. This may be due to the low crystalline quality of ZnO synthesized at low temperature [30].

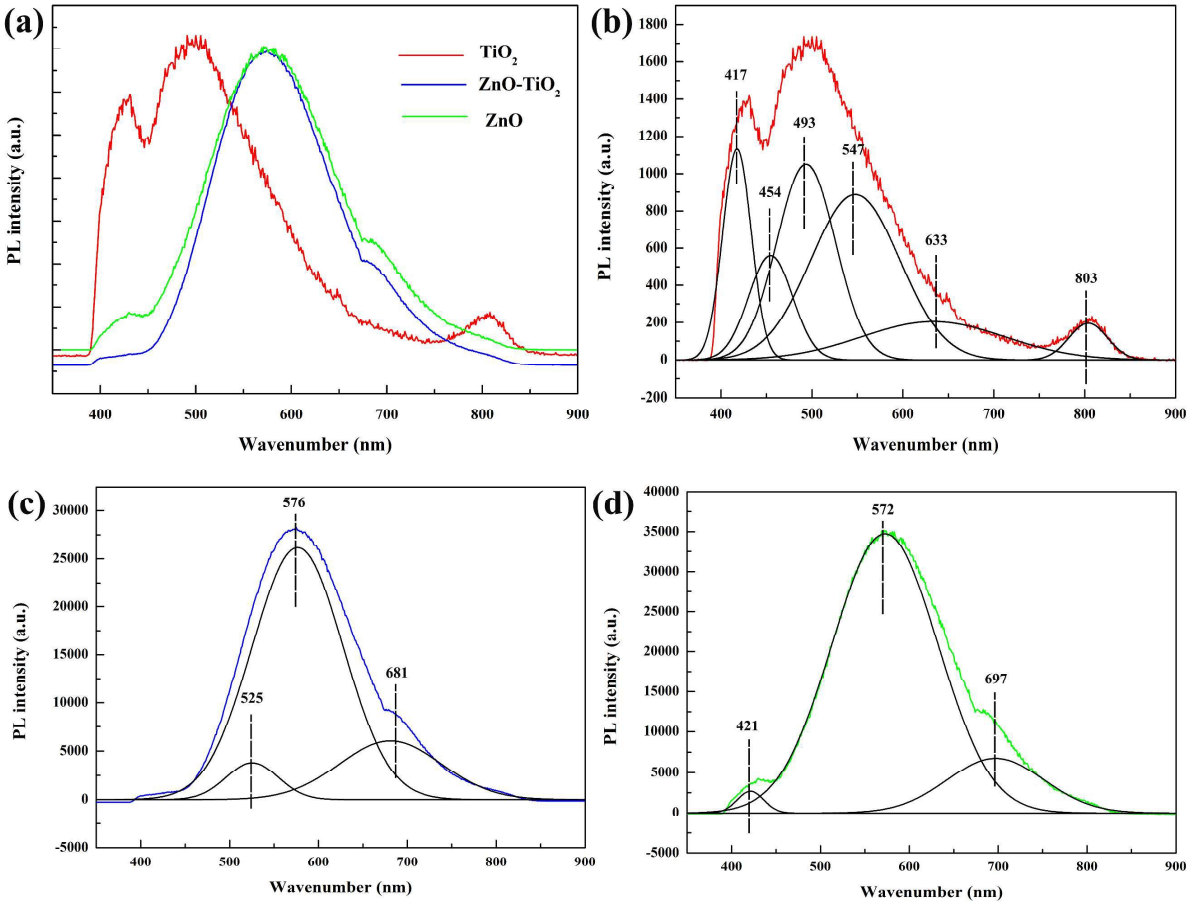

Fig. 8 (a) PL spectra for TiO_2 fibers, ZnO-TiO_2 heterostructure and ZnO NRs. (b) the curve fitting of the PL spectra for TiO_2 fibers, (c) ZnO-TiO_2 heterostructure, (d) ZnO NRs.

4. Conclusions

In summary, in a chemical bath deposition process, the surfaces of TiO_2 fibers were successfully functionalized by a sheath of ZnO NRs without using seed layers. The photoluminescence of the TiO_2 was quenched by the covered ZnO NRs. The NRs have robust adhesive strength with TiO_2 fibers that violent ultrasonic power could not peel off the ZnO NRs from the TiO_2 fibers. The seedless growth mechanism was clarified. It indicates that TiO_2 fibers became electronegative in ZnO growth solution in which a Zn-based layer double hydroxide, named $Zn_5(OH)_8(NO_3)_2 \cdot 2H_2O$, was formed. As a precursor, Zn_5 with electropositive nature could be easily absorbed on the fibers surface due to electrostatic attraction. With increasing temperature, Zn_5 was transformed into ZnO NRs whose growth directions were nearly perpendicular to fibers.

Associated Content

Supporting information

Synthesis of organotitanium compound, parameters of force-spinning process, photo image and XRD patterns of TiO_2 fibers heat-treated at 500 °C, magnified SEM image of ZnO NRs anchored on TiO_2 fibers, Zeta potential of ZnO growth solution and TiO_2 fiber aqueous solution, SEM image of oriented attachment growth found in the ZnO NRs homogeneously grown in growth solution

Acknowledgements

The authors acknowledge the financial support of the National Natural Science Foundations of China (Grant Nos. 51472144, 51372140 and 51102155), and the Fundamental Research Funds of Shandong University (Grant no. 2015JC022). In addition, the authors thank Qian Gu from Department of Art and Crafts, Shandong Technician Institute, for her help of schematic drawing.

Reference

1. A. Pimentel, D. Nunes, P. Duarte, J. Rodrigues, F. M. Costa, T. Monteiro, R. Martins and E. Fortunato, *J. Phys. Chem. C.*, 2014, **118**, 14629-14639.
2. M. Pazoki, N. Nafari and N. Taghavinia, *RSC Adv.*, 2014, **4**, 301.
3. K. O. Iwu, V. Strano, A. Di Mauro, G. Impellizzeri and S. Mirabella, *Cryst. Growth. Des.*, 2015, **15**, 4206-4212.
4. Y. Qin, X. Wang and Z. L. Wang, *Nature*, 2008, **451**, 809-813.
5. A. Ghosh, P. Guha, A. K. Samantara, B. K. Jena, R. Bar, S. Ray and P. V. Satyam, *ACS. Appl. Mater. Inter.*, 2015, **7**, 9486-9496.
6. X. Du, X. Huang, X. Li, X. Meng, L. Yao, J. He, H. Huang and X. Zhang, *J. Collid. Interf. Sci.*, 2015, **458**, 79-86.
7. M. Suja, S. B. Bashar, M. M. Morshed and J. Liu, *ACS. Appl. Mater. Inter.*, 2015, **7**, 8894-8899.
8. C. Thiandoume, J. Barjon, O. Ka, A. Lusson, P. Galtier and V. Sallet, *J. Cryst. Growth.*, 2009, **311**, 4311-4316.

9. Y. Liu and W. Gao, *J. Alloy. Compd.*, 2015, **629**, 84-91.
10. C. Xu, J.-H. Lee, J.-C. Lee, B.-S. Kim, S. W. Hwang and D. Whang, *CrystEngComm.*, 2011, **13**, 6036.
11. Z. Yang, M. Wang, S. Shukla, Y. Zhu, J. Deng, H. Ge, X. Wang and Q. Xiong, *Sci. Rep.*, 2015, **5**, 11377. `
12. J. H. Kim, D. Andeen and F. F. Lange, *Adv. Mater.*, 2006, **18**, 2453-2457.
13. K. Govender, D. S. Boyle, P. O´Brien, D. Binks, D. West, and D. Coleman, *Adv. Mater.* 2002, **14**, 1221-1224.
14. Z. Zheng, Z. S. Lim, Y. Peng, L. You, L. Chen and J. Wang, *Sci. Rep.*, 2013, **3**, 2434.
15. Q. Li, X. Sun, K. Lozano and Y. Mao, *J. Phys. Chem. C.*, 2014, **118**, 13467-13475.
16. H. Liu, Y. Chen, S. Pei, G. Liu and J. Liu, *J. Sol-Ge. Sci. Technol.*, 2013, **65**, 443-451.
17. N. Nityashree and M. Rajamathi, *J. Phys. Chem. Solids.*, 2013, **74**, 1164-1168.
18. S. J. Ahmadi, M. Hosseinpour, F. Javadi and R. Tayebee, *Ind. Eng. Chem. Res.*, 2013, **52**, 1448-1454.
19. W. J. T. Biswick, A. Pacula, E. Serwicka, J. Podobinski., *J. Solid State Chem.*, 2007, **180**, 1171-1179.
20. M.-K. Liang, M. J. Limo, A. Sola-Rabada, M. J. Roe and C. C. Perry, *Chem. Mater.*, 2014, **26**, 4119-4129.
21. G. Arizaga, K. Satyanarayana and F. Wypych, *Solid State Ionics*, 2007, **178**, 1143-1162.
22. M. Wang, Y. Zhou, Y. Zhang, S. H. Hahn and E. J. Kim, *CrystEngComm.*, 2011, **13**, 6024-6026.
23. H. G. Liao, L. Cui, S. Whitelam, and H. Zhang, *Science.,* 2012, **336**, 1101-1104
24. A. P. Nayak, A. M. Katzenmeyer, Y. Gosho, B. Tekin and M. S. Islam, *Appl. Phys. A.*, 2012, **107**, 661-667.
25. L. Vayssieres, K. Keis, A. Hagfeldt and S. Lindquist, *Chem. Mater.*, 2001, 13, 4395-4398.
26. Y. Lei, L. D. Zhang, G. W. Meng, G. H. Li, X. Y. Zhang, C. H. Liang, W. Chen and S. X. Wang, *Appl. Phys. Lett.*, 2001, **78**, 1125-1127.
27. J. Shi, J. Chen, Z. Feng, T. Chen, Y. Lian, X. Wang and C. Li, *J. Phys. Chem.,* C. 2007,**111**,693-699
28. C. W. Zou, X. D. Yan, J. Han, R. Q. Chen, J. M. Bian, E. Haemmerle and W. Gao, *Chem. Phys. Lett.*, 2009, **476**, 84-88.
29. L. Shi, H. Shen, L. Jiang and X. Li, *Mater. Lett.,* 2007, **61**, 4735-4737.
30. E. Rauwel, A. Galeckas, P. Rauwel, M. F. Sunding and H. Fjellvag, *J. Phys. Chem. C.*, 2011, **115**, 25227-25233.

TOC

Seedless growth of ZnO nanorods on TiO_2 microfibers was reported, and the growth mechanism was demonstrated.